REPORT
SOLID EARTH: SEISMOLOGY

Earth and Planetary Physics
9: 467–473, 2025
doi: 10.26464/epp2025028

Rapid report of source characteristics of 2025 M_S6.8 Dingri, Xizang earthquake sequence

Wen Yang[1], Jie Liu[1*], ZhiGao Yang[1], Ran Cui[1], JinRui Gao[2], YanYan Han[1], HuaiZhong Yu[1], LingYuan Meng[1], and XueMei Zhang[1]

[1]China Eartquake Networks Center, Beijing 100045, China;

[2]Earthquake Administration of Xizang Autonomous Region, Lhasa 850000, China

Citation: Yang, W., Liu, J., Yang, Z. G., Cui, R., Gao, J. R., Han, Y. Y., Yu, H. Z., Meng, L. Y., and Zhang, X. M. (2025). Rapid report of source characteristics of 2025 M_S6.8 Dingri, Xizang earthquake sequence. *Earth Planet. Phys.*, *9*(2), 467–473. http://doi.org/10.26464/epp2025028

Abstract: Characteristics of the main shock and aftershocks of the Dingri M_S6.8 earthquake in the Xizang Autonomous region were determined by the double-difference location method using phase reports from Jan. 7 to Jan. 16, 2025. We find that the aftershocks were generally distributed in a near NS direction along the Dengmoduo fault, with a long axis of about 70 km. There is an obvious seismic gap to the north side of the main shock, which is consistent with the location of the maximum rupture point as revealed by surface survey of the rupture and inversion analysis of the rupture process. In addition, the aftershock distribution exhibits obvious north–south segmentation characteristics. These observations suggest that the seismic fault of the main shock was likely to have been the Dengmoduo fault, which is NS and slightly inclined to the west.

Keywords: Dingri M_S6.8 earthquake; Double-difference location; aftershock activity; Dengmoduo fault

1. Introduction

According to the China Earthquake Networks Center (CENC), at 9:05 on January 7, 2025, Beijing time, a strong earthquake of M_S6.8 and focal depth of 10 km occurred in Dingri County (87.45°E, 28.50°N), Shigatse city, in the south part of the Xizang Autonomous region. This earthquake occurred to the south of the Yarlung Zangbo River suture zone on the southwestern margin of the Himalayas, and on the west side of the Dengmoduo fault in the southern section of the Xainza–Dinggye fault system within the southern Tibet rift system (Figure 1). In the area around the Dingri epicenter, a series of NS-striking extensional tectonic systems, including the Xainza–Dinggye fault system, have developed due to the east–west extension that occurred during the convergence of the Indian and Eurasian plates. The Xainza–Dinggye fault system starts from the south of Shenzha County at the Jiagang snowy mountain in the north, runs southward through Xietongmen County, crosses the Yarlung Zangbo River, and extends to the north of Dingjie County, cutting through the southern Tibet detachment zone (Zhang JJ et al., 2002, 2007; Xu XY, 2019). The Xainza–Dinggye fault system can be divided into three sections: the northern section of the Yarlung Zangbo River suture zone, which is mainly a brittle normal fault dipping to ESE; the middle section from the Yarlung Zangbo River suture zone to the southern Tibet detachment zone, which is a normal fault dipping to WNW; and the southern section of the southern Tibet detachment zone, which is a detachment fault dipping to ESE (Zhang XT et al., 2020). The Dengmoduo fault is a nearly north–south trending normal fault with a length of 60 km and a width of 30–300 m; it has been active since the beginning of the Holocene (Liu DS and Li M, 2024).

Since 1900, a total of 19 earthquakes of magnitude 6.0 and above have occurred within 300 km of the Dingri epicenter (Figure 1b), including one earthquake of M_S8.0–8.9, two of M_S7.0–7.9, and 16 of M_S6.0–6.9. The most recent previous earthquake of M_S6.0 or above was the Dingri M_S6.2 earthquake on Sep. 4, 1998; its epicenter was about 15 km from the epicenter of the 2025 Dingri earthquake. The largest earthquake since 1900 in this region was the M_S8.1 earthquake in Nepal on Apr. 25, 2015, about 270 km away, after which the number of M_S4.0 earthquakes or above in the vicinity of Dingjie County and along the Dengmoduo fault increased significantly, suggesting that the 2015 Nepal earthquake had a significant role in promoting the activity of the Dengmoduo fault (Tian TT and Wu ZH, 2023).

According to the earthquake intensity map released by the China Earthquake Administration of the Ministry of Emergency Management (http://www.cea.gov.cn/cea/xwzx/fzjzyw/5790712/index.html), the Dingri earthquake caused a surface rupture of about 26 km; its highest intensity reached level IX (China Earthquake Intensity Scale, GB/T 17742-2020) and affected an area of approximately 411 km^2. This strong earthquake caused a large loss of personnel and property. As of January 16, 126 people had been reported killed by the earthquake. The quake's isoseismic line distribution is generally oval in shape, its long axis trending nearly

First author: W. Yang, yangwen@seis.ac.cn
Correspondence to: J. Liu, liujie@seis.ac.cn
Received 13 JAN 2025; Accepted 02 MAR 2025.
First Published online 05 MAR 2025.

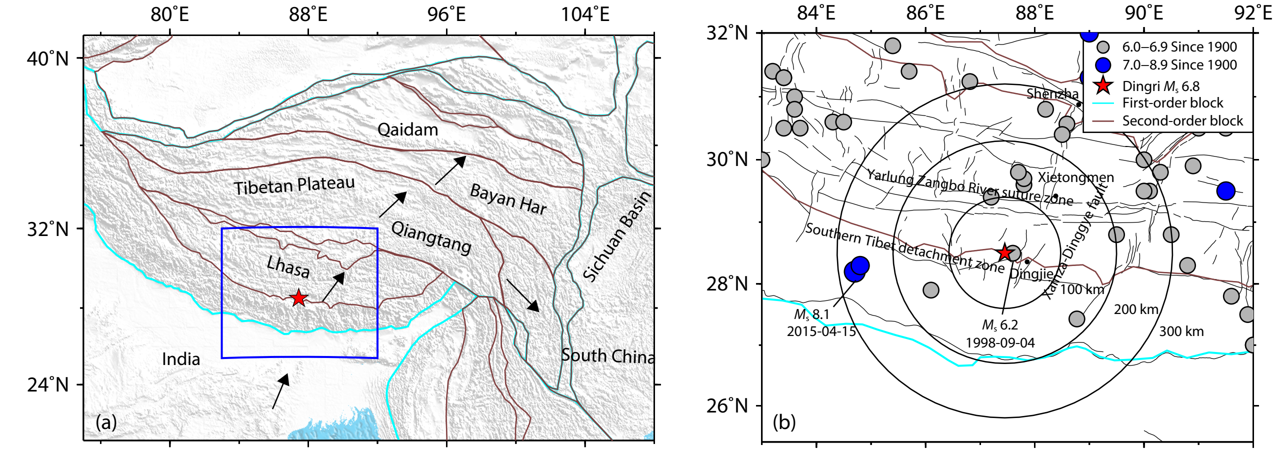

Figure 1. Tectonic setting and historical earthquake distribution map of the region surrounding Dingri.

NS. In the region of VI intensity, the long axis appears to have been about 191 km; the short axis, about 152 km. Inversion of the rupture process produced by CENC concludes that the earthquake was dominated by unilateral rupture, and that the rupture surface is in the NS direction. The rupture duration is estimated for have been about 27 s with a length of about 55 km. The rupture extends mainly northward from the epicenter; the maximum rupture point is located 30 km north of the epicenter with a slip of 1.4 m (https://data.earthquake.cn/gxdt/info/2025/334672994.html). In this paper, we seek to relocate the main shock and aftershocks of this event by applying the double-difference location method (Waldhauser and Ellsworth, 2000) to data in the phase report provided by the CENC. The relocation provides a preliminary description of the spatial and temporal evolution of the earthquake sequence. These details will support subsequent assessment of seismic activity in this region as well as contribute to improve research in this field in general.

2. Focal Mechanism of the Main Earthquake and Characteristics of the Aftershock Activity

Table 1 gives the focal mechanism solution, moment magnitude, latitude and longitude, and centroid depth of the main shock as reported by various agencies around the world. The focal mechanism results released by each agency are generally consistent, indicating that the earthquake occurred on a normal fault (Figure 2a).

According to the earthquake catalog provided by Xizang Regional Seismic Network (XRSN), as of 24:00 on January 16, 2025, a total of 4416 aftershocks were recorded in the Dingri M_S6.8 earthquake sequence, including 1879 events of M_L1.0–1.9, 2187 events of M_L2.0–2.9, 257 events of M_L3.0–3.9, and 8 events of strength M_S4.0 and greater. The largest aftershock was the Dingri M_S5.0 earthquake at 20:58 on January 13 (Table 2). As shown in Figure 2a, these aftershocks were distributed mainly along the Dengmoduo fault, ranging primarily through Dingri, Dingjie, Lazi counties, and so on.

According to the Gutenberg–Ricker relationship (Figure 2b), the *b* value of the earthquake sequence fitted by the maximum likelihood method is about 1.1, and its minimum completeness magnitude is about M_L2.5. According to the *M-t* diagram of the Dingri M_S6.8 earthquake sequence (Figure 2c), its aftershock activity was relatively abundant. The aftershocks showed fluctuating activity characteristics, and the aftershock magnitude level is about 5.0.

3. Relocation of the Earthquake Sequence

In this study, the seismic phase report of the XRSN was used to relocate the Dingri M_S6.8 earthquake sequence by applying the double-difference location method, and seismic events from Jan. 7 to Jan. 16, 2025 were selected. The broadband seismic stations of the XRSN are relatively sparse; only two broadband seismic stations are within 200 km of the Dingri earthquake epicenter.

Table 1. Focal mechanism solution of M_S6.8 earthquake released by different agencies.

Origin	M_W	Depth (km)	Longitude (E°)	Latitude (N°)	Strike1/Dip1/Rake1 (°)	Strike2/Dip2/Rake2 (°)
CENC[1]	7.1	10	87.45	28.50	348/40/−100	181/51/−81
GCMT[2]	7.1	12	87.47	28.56	356/42/−88	173/48/−92
GFZ[3]	7.1	14	87.40	28.56	164/41/−102	0/49/−79
USGS[4]	7.1	11.5	87.36	28.64	349/42/−103	187/49−78
IGP[5]	7.0	10	87.45	28.50	346/49/−95	174/42/−85

[1]https://data.earthquake.cn/datashare/report.shtml?PAGEID=earthquake_dzzyjz
[2]http://www.globalcmt.org/CMTsearch.html
[3]https://geofon.gfz.de/eqinfo/event.php?id=gfz2025albe
[4]https://earthquake.usgs.gov/
[5]https://www.cea-igp.ac.cn/kydt/280883.html

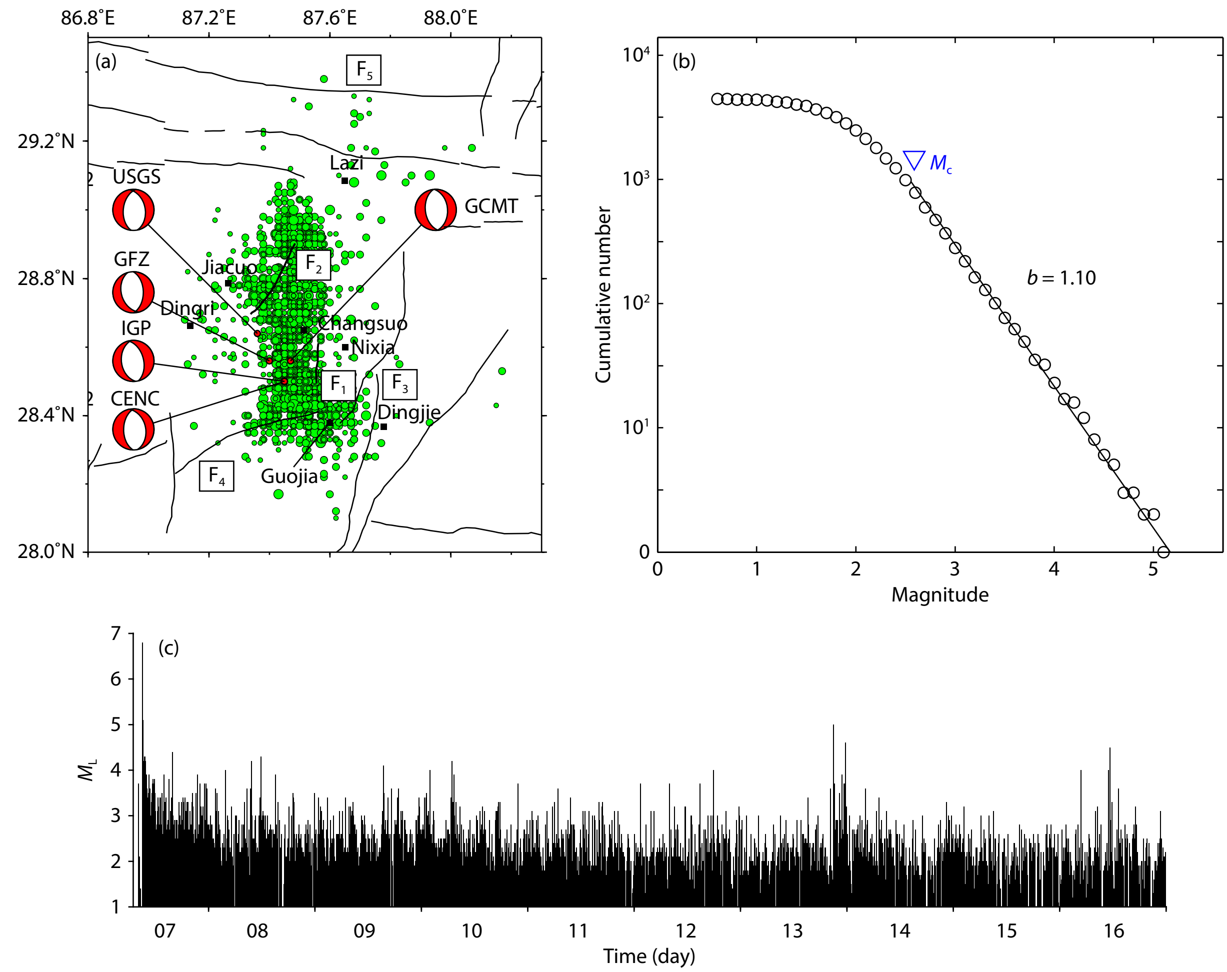

Figure 2. (a) The distribution of Dingri earthquake sequence; (b) magnitude–frequency relationship diagram; and (c) *M-t* diagram. The magnitude scale is the M_L. The red circles in Figure2a indicate the main shock locations as determined by data collected by different seismic observing stations; the green circles indicate the aftershocks; thick black line F_1 , Dengmoduo fault; thick black line F_2, Northern section of Dengmoduo fault; thin black line F_3, Xainza–Dinggye fault; thin black line F_4, Southern Tibet detachment fault; thin black line F_5, Yarlung Zangbo River fault.

Table 2. Catalog of Dingri main shock and strong aftershock above M_S4.0.

Number	Date	Beijing time (GMT+8)	Latitude (°N)	Longtitude (°E)	M_S	Depth (km)	Place
1	2025/1/7	9:05:16	28.50	87.45	6.8	10	Dingri County, Shigatse City, Xizang
2	2025/1/7	9:24:26	28.35	87.37	4.4	10	Dingri County, Shigatse City, Xizang
3	2025/1/7	9:37:12	28.36	87.67	4.2	10	Dingjie County, Shigatse City, Xizang
4	2025/1/7	9:43:48	28.22	87.63	4.1	10	Dingjie County, Shigatse City, Xizang
5	2025/1/8	11:51:20	28.42	87.44	4.0	10	Dingri County, Shigatse City, Xizang
6	2025/1/13	20:57:36	28.42	87.50	4.9	10	Dingri County, Shigatse City, Xizang
7	2025/1/13	20:58:20	28.45	87.52	5.0	10	Dingri County, Shigatse City, Xizang
8	2025/1/13	23:44:42	28.47	87.50	4.2	10	Dingri County, Shigatse City, Xizang
9	2025/1/16	11:19:58	28.47	87.50	4.4	10	Dingri County, Shigatse City, Xizang

However, at 0:40 on January 9, after the Dingri M_S6.8 earthquake, the Earthquake Administration of Xizang Autonomous Region set up a number of temporary stations (Figure 3) around the source area. These added stations provided rich data support for this study of the seismogenic structure of the earthquake sequence. We selected P and S wave phase arrivals recorded by 28 stations within 400 km of the epicenter location, including by the temporary stations; each event chosen was required to have at least 4 recorded phases. The linear least squares fitting was performed between the distance and the travel time; candidate events for which data exhibited obvious anomalies (exceeding 5 s) were eliminated. Finally, 25724 P waves and 25994 S waves were

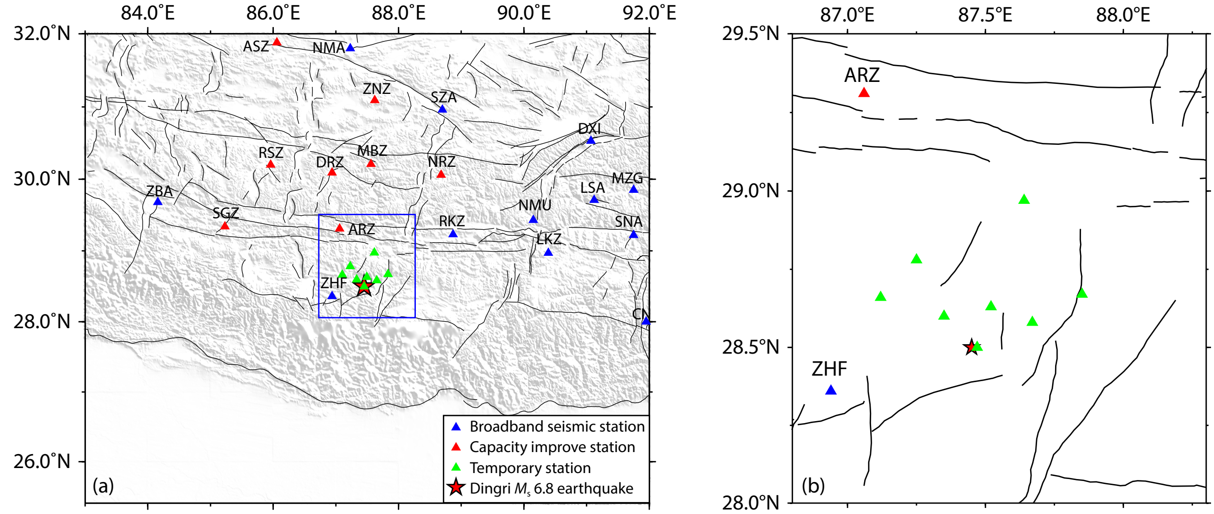

Figure 3. The Dingri M_S6.8 earthquake and the stations used (a) and the temporary stations around source (b).

selected. In the inversion, the P-wave arrivals were assigned a weight of 1.0; the S-wave data were given a weight of 0.5. The maximum distance between earthquake pairs was set to no more than 20 km; to be considered a cluster (OBSCT), the minimum number of catalog links per event pair was set to 8. The velocity model uses the results of Crust2.0 (Bassin et al., 2000), which is divided into four layers, as shown in Table 3. In this study, the V_p/V_s ratio was set to 1.71. The conjugate gradient method was used to solve the equation; two groups of 10 interations were performed to reach the damped least squares solution.

After relocation, we obtained source location parameters of 3339 earthquakes. The relocated epicenter of the main shock is 28.494°N, 87.502°E; its focal depth is 8.6 km. The focal depth of the aftershocks is found to be concentrated primarily in the 6–12 km layer; average aftershock depth is 10.4 km (Figure 4).

The relocated epicenter and aftershock distribution (Figure 4a) is clearly more concentrated than is seen in Figure 2a; its linear trend is also more obvious. In the horizontal direction, the Dingri M_S6.8 main shock is located in the south of the aftershock zone. The aftershocks are generally distributed over a long axis (marked AA' in Figure 4a) stretching about 70 km in the NS direction along the Dengmoduo fault. The aftershock area is characterized by obvious segmentation that can be divided into roughly two segments: northern and southern. The aftershocks in the southern part are concentrated in roughly the NW direction whereas aftershocks in the northern part are obviously distributed along the NNE direction (Figure 4a). Moreover, the southern section experienced relatively higher numbers and intensities of aftershocks above M_L4.0 than were observed in the northern section. An obvious seismic gap of about 10 km, north of the main shock, can be seen between the two sections. The long axis of the northern section is about 35 km; that of the southern section is about 25 km.

Table 3. The initial one-dimensional P-wave velocity model for the Dingri region.

Depth of upper surface (km)	0	22	46	70
Velocity of P wave (km·s^{-1})	4.0	6.0	6.4	7.1

The depth profile along the line AA' (Figure 4b) shows that the main shock and the aftershocks above M_L4.0 are shallower, which may be one of the reasons for the serious disasters. The inversion result of the rupture process reveal that the maximum rupture point is located at 30 km north of the main shock (https://www.cea.gov.cn/cea/xwzx/365134/5790366/index.html), which is in the area where the earthquake caused the most casualties, and is also in good agreement with the location of the seismic gap. The main shock rupture zone and aftershock distribution of the 2014 Yutian M_S7.3 earthquake in Xinjiang and the 2022 Luding M_S6.8 earthquake in Sichuan also showed similar phenomena (Tang MS et al., 2016; Yang W et al., 2022; Yang ZG et al., 2022); this pattern suggests that most of the stress in the main rupture zone was released during the main shock. Along the BB' direction (Figures 4a and 4c), the distribution of the aftershocks exhibits a linear trend with fault dip angle westward; the dip angle is about 50°–70°, which is consistent with the fault properties of the Dengmoduo fault (Liu DS and Li M, 2024). The CC', DD' and EE' cross sections (Figure 4d, 4e, 4f) show that the aftershocks in the southern segment are deep in the west and shallow in the east and do not exhibit obvious linear characteristics, suggesting that the southern segment may be affected by other faults besides the Dengmoduo fault.

Figure 5 presents the distribution and depth profile of the earthquake sequence from 20:57 to 24:00 on January 13 that followed the M_S4.9 and M_S5.0 earthquakes. The spatial distribution (Figure 5a) of these two quakes and subsequent smaller earthquakes reveals that they are distributed mainly along the NNW direction, with a strike of nearly 180°. The focal depth of the earthquakes during this time was shallow (mostly within 10 km). Along different depth profiles (Figure 5b, 5c, 5d), the distribution of small earthquakes in the FF' section is generally more dispersed; those in the GG' and HH' sections are more concentrated, indicating that the M_S4.9 and M_S5.0 earthquakes may have been controlled by shallow NNW branch faults.

In order to better understand the expansion pattern of the after-

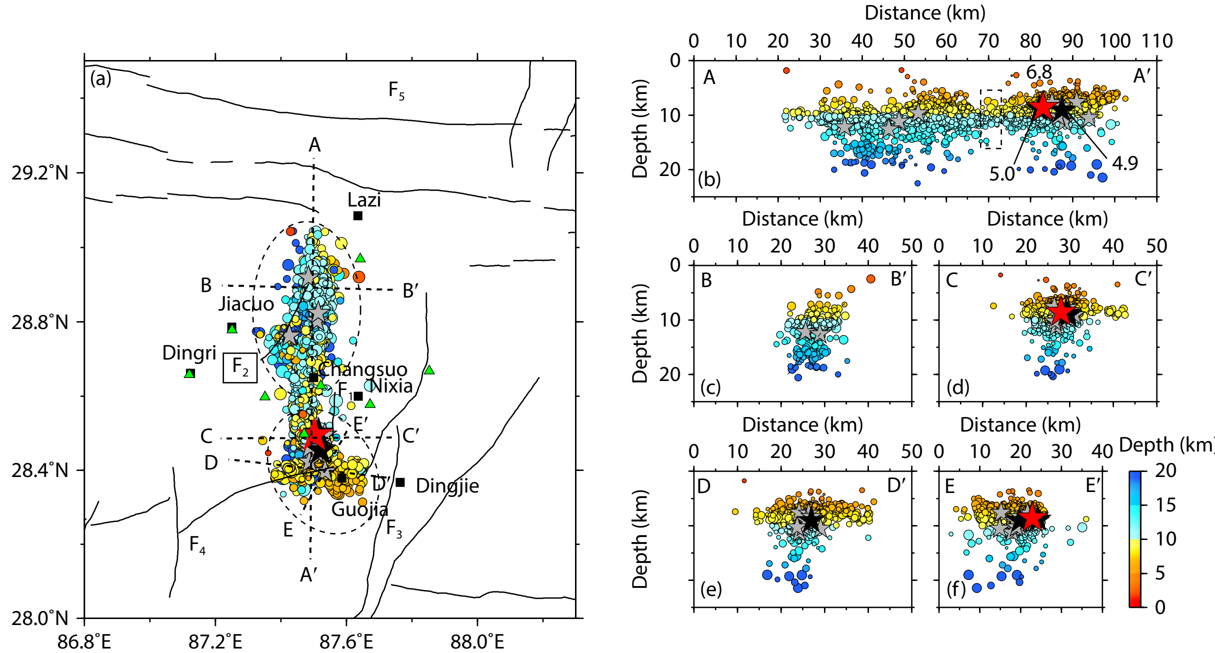

Figure 4. Distribution and depth profiles of the Dingri M_S6.8 earthquake sequence after relocation. The red star indicates the M_S6.8 main shock; black stars indicate M_S5.0 and M_S4.9 aftershocks; the gray stars indicate other aftershocks of M_L4.0 and above. In Figure (a), green triangles indicate temporary stations set up after the main shock; the dashed circles indicate the range of the northern and southern sections of the aftershock zone in Figure 7. The dashed retangle in Figure (b) is the location of the seismic gap. The thick dotted line in Figure (c) is the presumed fault location.

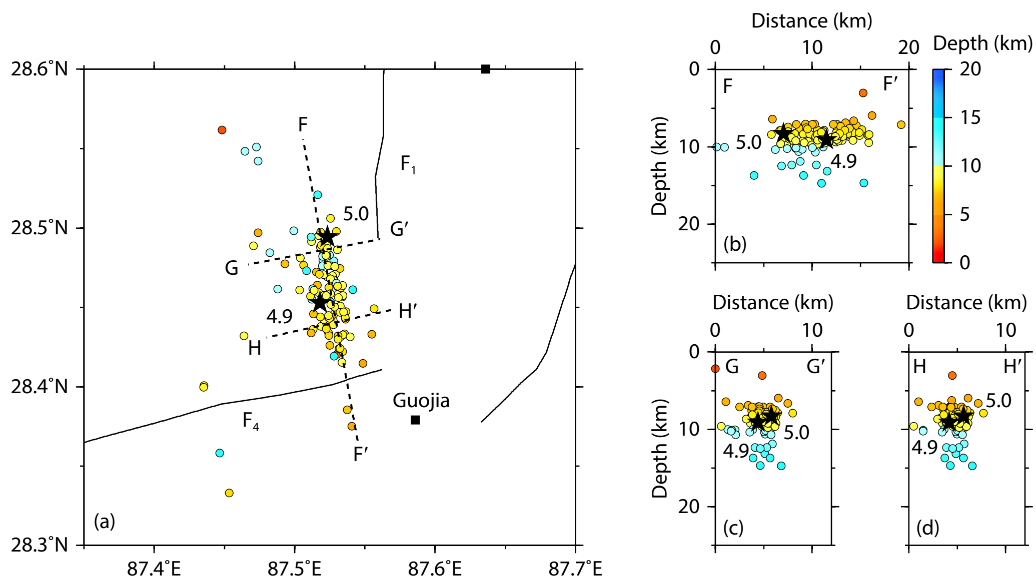

Figure 5. Relocated distribution and depth profile of the aftershock sequence from 20:57 to 24:00 on January 13, 2025 that followed the M_S4.9 and M_S5.0 earthquakes.

shocks, we drew a distribution map of aftershocks in different time periods after the main shock. The aftershocks 0–2 hours after the main shock occurred on both sides of Changsuo Town; they were distributed generally in the NS direction along the Dengmoduo fault. To the north of the main shock, aftershocks were distributed along the NNE direction of the northern section of the Dengmoduo fault. An obvious seismic gap appears near Changsuo Town (Figure 6a); the surface rupture survey shows that this is the section with the largest surface rupture (Shi F et al., 2025), indicating that the main shock may have ruptured sufficiently to relieve most stress in this area. Aftershocks to the south of the main shock extended northward to the vicinity of Changsuo Town. As time passed, aftershocks along the northern section gradually expanded outward; the seismic gap in the north of Changsuo Town, however, was still apparent 2–6 hours after the main shock (Figure 6b). The aftershocks continued to move NS; the seismic gap near Changsuo Town began to be filled to a certain extent; the aftershocks in the southern section slightly expanded toward the south; and 6–12 hours after the main shock the aftershock range increased slightly. During this period, an M_L4.4 earthquake occurred near Guojia Town in the southern section of the aftershock zone (Figure 6c). The aftershock distribution was still quite obviously oriented NS, and the seismic activity near Changsuo Town was still weak, with the seismic gap emerging again 12–24 hours after the main shock (Figure 6d). The aftershocks were still distributed within the previous aftershock zone 24 hours to 3 days after the main shock. In the northern section, the aftershock distribution was primarily along the NNE direction; to the south, aftershocks were distributed along the SE direction. A cluster of earthquakes with maximum magnitude of M_L4.3 occurred in the northern part of Guojia Town; seismic activity in the southern section was more distinctly shallow (Figure 6e) than in the north. Three days after the main shock, aftershock activity continued with no obvious expansion phenomenon — aftershocks remained within the previous range. During this period, strong aftershocks of M_S4.9 and M_S5.0 occurred continuously near the main shock (Figure 6f). These facts lead us to conclude that the activity of this earthquake sequence was controlled mainly by the Dengmoduo fault, but with aftershocks that exhibit significantly different activity characteristics in the north compared to the south.

Focal depth is an important parameter in analyzing seismogenic structures (Yang ZG et al., 2024). The variation of focal depth over time is of great significance for detailed analysis of earthquake sequence and rupture progression. The focal depths of the southern and northern segments of the Dingri M_S6.8 earthquake sequence have different temporal characteristics (Figure 7). On the day of the main shock, January 7, the depth range of aftershocks was broad, from 5–20 km. As time went on, especially after January 9, analysis of the aftershocks in the north and southern segments shows a significant trend toward shallowing and concentration in depth, but this may be partly or wholly artefactual, related to the increase in data from the temporary stations.

After the 9th, the focal depths of the northern segment were relatively dispersed, mainly concentrated between depths of 5–15 km, while in the southern segment the concentration was at 5–10 km. Seismic activity above M_L4.0 was weak in the northern segment; in the southern segment, the depths of earthquakes M_L4.0 and greater were more concentrated, fluctuating mainly near 10 km.

4. Conclusion

This paper is based on phase report data recorded by the XRSN. We applied the double-difference location method to relocate the Dingri M_S6.8 main shock and its aftershock sequence from January 7 to 13, 2025. The accuracy of the relocation results is much higher than preliminary results from the XRSN. The following preliminary understandings are obtained: (1) The epicenter of the relocated main shock is 28.494°N, 87.502°E; its focal depth is about 8.6 km. The focal depths of the aftershocks are distributed mainly over 6–12 km with an average depth of 10.4 km. (2) The

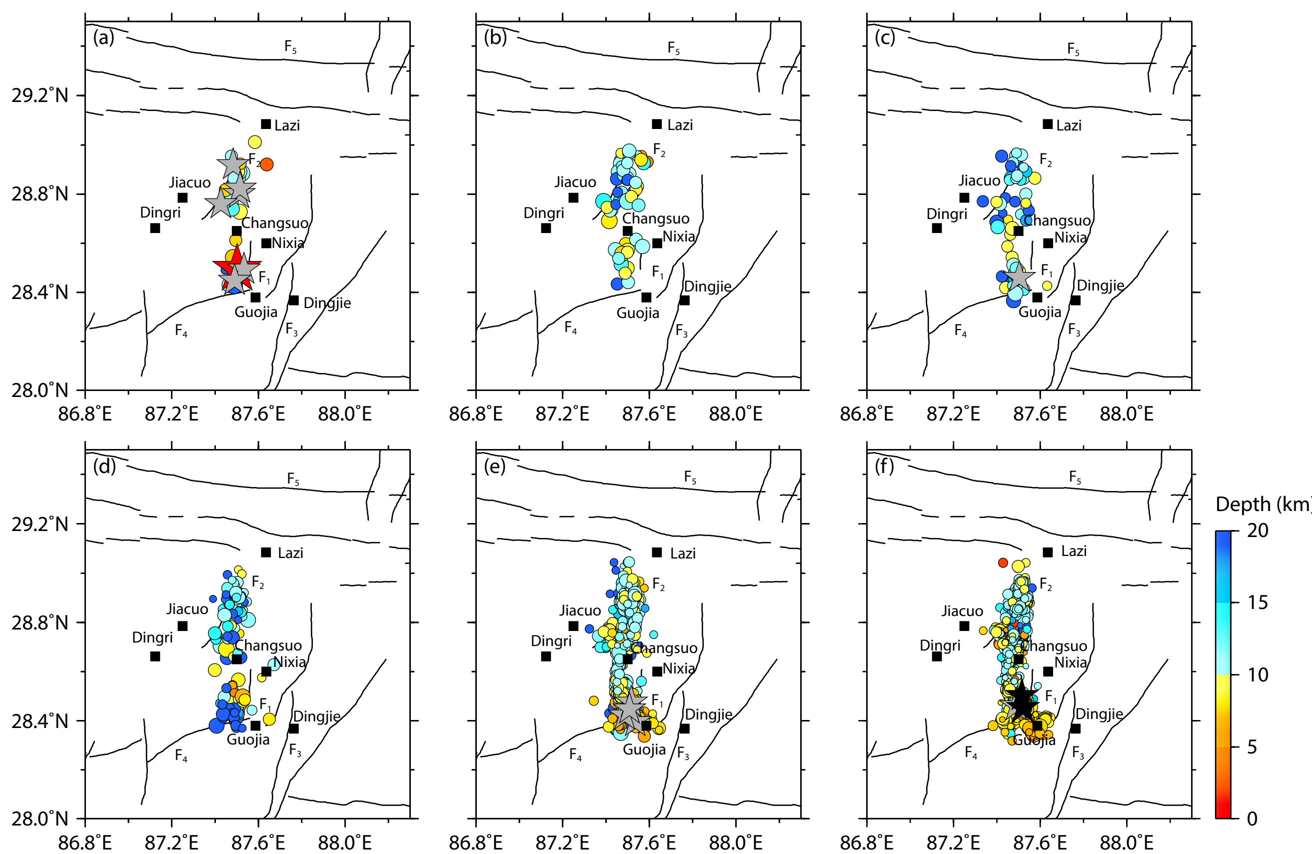

Figure 6. The spatial expansion of aftershocks of Dingri M_S6.8 earthquake. (a) 0–2 hours; (b) 2–6 hours; (c) 6–12 hours; (d) 12–24 hours; (e) 24 hours–3 days; and (f) >3 days. The red star indicates the M_S6.8 main shock, the black stars indicate M_S5.0, and M_S4.9 aftershocks, and the gray stars indicate other aftershocks at or above M_L4.0.

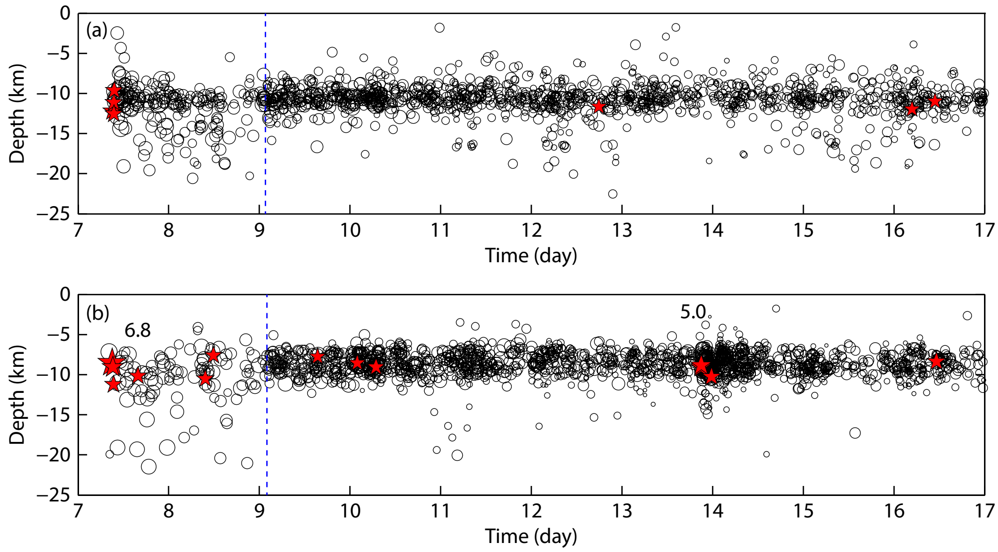

Figure 7. Time-dependent depth map of the aftershock sequence of the Dingri M_S6.8 earthquake. (a) Northern segment; and (b) southern segment. The red stars indicate the M_S6.8 main shock and the aftershocks above M_L4.0. The blue dotted lines in (a) and (b) indicate the times when the temporary stations began to set up.

aftershocks during the period covered by our data appear to have been distributed primarily in a nearly NS direction for about 70 km along the Dengmoduo fault. There is an obvious seismic gap to the north of the main shock, which is consistent with the location of the maximum rupture point revealed by the inversion results of the rupture process. (3) The distribution of the aftershocks shows an obvious north−south segmentation. The aftershocks in the southern section are relatively concentrated and tend to move towards the SE direction. The aftershocks in the northern section are distributed along the NNE direction. The fault is slightly inclined to the west as a whole, and the seismogenic fault of the main shock was likely the Dengmoduo fault.

Data and Resources

The earthquake catalog and the phase data were provided by the CENC. The temporary station data was provided by the Earthquake Administration of Xizang Autonomous Region. Most of the figures in this paper were drawn using GMT software (Wessel et al., 2019). This study was sponsored by National Key R&D Program of China (No. 2023YFC3012005-3, No.2018YFE0109700), Earthquake Joint Funds of NSFC (No. U2039205) and Task of earthquake monitoring, forecasting and early warning, China Earthquake Adminstration (CEA-ZQGZ-202501059). We thank the reviewers for comments and suggestions that improved this manuscript.

References

Bassin, C., Laske, G., and Masters, G. (2000). The current limits of resolution for surface wave tomography in North America. *Eos, Trans. Am. Geophys. Union*, *81*, F897.

Liu, D. S., and Li, M. (2024). Characteristics of active faults and their engineering influence analysis in domestic section of Shigatse-Jilong railway. *Sci. Technol. Eng. (in Chinese)*, *24*(17), 7327–7333. https://doi.org/10.12404/j.issn.1671-1815.2301728

Shi, F., Liang, M. J., Luo, Q. X., Qiao, J. X., Zhang, D., Wang, X., Yi, W. X., Zhang, J. W., Zhang, Y. F., … Li, A. (2025). Seismogenic fault and coseismic surface deformation of the Dingri M_S6.8 earthquake in Tibet, China. *Seismol. Geol. (in Chinese)*, *47*(1), 1–15. https://doi.org/10.3969/j.issn.0253-4967.2025.01.001

Tang, M. S., Wang, H. T., Li, Y. Y., Reyi, M. J., Kong, X. Y., Wei, Y. Y., Shangguan, W. M., and Wei, B. (2016). Relocation of the 2014 Yutian, Xinjiang, M_S7.3 earthquake sequence and a preliminary study of its seismogenic structure. *Chin. J. Geophys. (in Chinese)*, *59*(6), 2126–2137. https://doi.org/10.6038/cjg20160618

Tian, T. T., and Wu, Z. H. (2023). Recent prehistoric major earthquake event of Dingmucuo Normal fault in the southern segment of Shenzha-Dingjie Rift and its seismic geological significance. *Geol. Rev. (in Chinese)*, *69*(S1), 53–55. https://doi.org/10.16509/j.georeview.2023.s1.020

Waldhauser, F., and Ellsworth, W. L. (2000). A double-difference earthquake location algorithm: Method and application to the northern Hayward Fault, California. *Bull. Seismol. Soc. Am.*, *90*(6), 1353–1368. https://doi.org/10.1785/0120000006

Wessel, P., Luis, J. F., Uieda, L., Scharroo, R., Wobbe, F., Smith, W. H. F., and Tian, D. (2019). The generic mapping tools version 6. *Geochem. Geophys. Geosyst.*, *20*(11), 5556–5564. https://doi.org/10.1029/2019GC008515

Xu, X. Y. (2019). Late Quaternary activity and its environmental effects of the N-S trend Kharta fault in Xainza-Dinggye rift, southern Tibet. Beijing: Institute of Geology, China Earthquake Administration. https://doi.org/10.27489/d.cnki.gzdds.2019.000038

Yang, W., Liu, J., Xie, M. Y., Zang, Y., Meng, L.Y., and Zhang, X. M. (2022). Study on Relocation of the September 5, 2022 Luding M_S6.8 earthquake. *Earthquake Res. China (in Chinese)*, *38*(4), 622–631. https://doi.org/10.3969/j.issn.1001-4683.2022.04.003

Yang, Z. G., Dai, D. Q., Zhang, Y, Zhang, X. M., and Liu, J. (2022). Rupture process and aftershock focal mechanisms of the 2022 *M*6.8 Luding earthquake in Sichuan. *Earthquake Sci.*, *35*(6), 474–484. https://doi.org/10.1016/j.eqs.2022.12.005

Yang, Z. G., Liu, J., Zhang, Y. Y., Yang, W., and Zhang, X. M. (2024). Rapid report of source parameters of 2023 *M*6.2 Jishishan, Gansu earthquake sequence. *Earth Planet. Phys.*, *8*(2), 436–443. https://doi.org/10.26464/epp2024012

Zhang, J. J., Guo, L., and Ding, L. (2002). Structural characteristics of middle and southern Xainza-Dinggye Normal Fault System and its relationship to southern Tibetan Detachment System. *Chin. Sci. Bull.*, *47*(13), 1063–1069. https://doi.org/10.1360/02tb9239

Zhang, J. J. (2007). A review on the extensional structures in the northern Himalaya and southern Tibet. *Geol. Bull. China (in Chinese)*, *26*(6), 639–649. https://doi.org/10.3969/j.issn.1671-2552.2007.06.003

Zhang, X. T., Jiang, X. H., Xue, Y., Yao, Q., Xie, M. Y., Zang, Y., Song, J., Lu, X., Yu, C., … Tian, L. (2020). Summary of the Dingri M_S 5.9 earthquake in Tibet on March 20, 2020. *Seismol. Geomagnetic Obs. Res.* (in Chinese), *41*(4), 193–203. https://doi.org/10.3969/j.issn.1003-3246.2020.04.024